EXTRATROPICAL WEATHER SYSTEMS ON MARS: RADIATIVELY-ACTIVE WATER ICE CLOUD EFFECTS.

J.L. Hollingsworth, M.A. Kahre, R.M. Haberle, *Space Science and Astrobiology Division, Planetary Systems Branch, NASA Ames Research Center, Moffett Field CA 94035 USA (jeffery.l.hollingsworth@nasa.gov)*, **R.A. Urata,** *BAER Institute/NASA Ames Research Center, Moffett Field CA 94035 USA*, **F. Montmessin,** *Laboratoire Atmosphères Mileux, Observations Spatiales (LATMOS), 78280 Guyancourt FR*.

Introduction: Extratropical, large-scale weather disturbances, namely transient, synoptic-period, baroclinic-barotropic eddies – or – low- (high-) pressure cyclones (anticyclones), are components fundamental to global circulation patterns for rapidly rotating, differentially heated, shallow atmospheres such as Earth and Mars. Such "wave-like" disturbances that arise via (geophysical) fluid shear instability develop, mature and decay, and travel west-to-east in the middle and high latitudes within terrestrial-like planetary atmospheres. These disturbances serve as critical agents in the transport of heat and momentum between low and high latitudes of the planet. Moreover, they transport trace species within the atmosphere (e.g., water vapor/ice, other aerosols (dust), chemical species, etc).

Figure 1: MGS/MOC hemispheric image analyses [*Wang et al.*, 2005] of large-scale synoptic extratropical weather systems during NH autumn and late winter with sequestered dust activity within cyclones/frontal waves.

Between early autumn through early spring, middle and high latitudes on Mars exhibit strong equator-to-pole mean temperature contrasts (i.e., "baroclinicity"). Data collected during the Viking era and observations from both the Mars Global Surveyor (MGS) and Mars Reconnaissance Orbiter (MRO) indicate that such strong baroclinicity supports vigorous, large-scale eastward traveling weather systems [*Banfield et al.*, 2004; *Barnes et al.*, 1993]. A good example of traveling weather systems, frontal wave activity and sequestered dust activity from MGS/MOC image analyses is provided in Figure 1 (cf. *Wang et al.* [2005]).

Utilizing an upgraded and evolving version of the NASA Ames Research Center (ARC) Mars global climate model, investigated here are key dynamical and physical aspects of simulated northern hemisphere (NH) large-scale extratropical weather systems, with and without radiatively-active water ice clouds.

Mars Climate Model: Over the past 5+ years, several major improvements have been made to the NASA ARC Mars global climate model (Mars GCM) to enhance its capabilities and to standardized its infrastructure. Physics improvements include an updated radiation code based on a generalized two-stream approximation for radiative transfer in vertically inhomogeneous multiple-scattering atmospheres [*Toon et al.*, 1989], together with a correlated-k method for calculating gaseous opacities [*Lacis and Oinas*, 1991]. In applications here, the radiation code responds to a prescribed dust distribution based on an opacity climatology derived from MGS Thermal Emission Spectrometer (TES) 9-μm opacity measurements during MY24. The vertical distribution varies with season and latitude.

A complex cloud microphysics package has been included based on the work of *Montmessin et al.* [2002]; *Montmessin et al.* [2004]. This microphysics module assumes a log-normal particle size distribution whose first two moments are carried as tracers, and which includes the nucleation, growth and sedimentation of ice crystals [*Montmessin et al.*, 2004]. The cloud microphysics package includes a time-splitting (sub-stepping) prognostic algorithm, and it interacts with a transported dust tracer whose surface source is adjusted to maintain an atmospheric column abundance as observed by TES. Aerosols of dust and water ice, in addition to water vapor, can be separately or collectively either radiatively inert (default case) or radiatively active (in combination). Other improvements in the climate model include implementing a new planetary boundary layer (PBL)
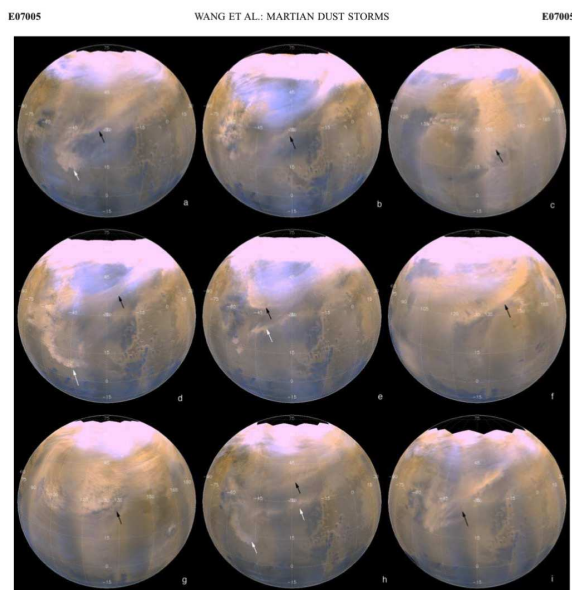
model (i.e., a level-2 Mellor and Yamada approach [*Mellor and Yamada*, 1982]; incorporation of a sub-surface land model; utilization of a highly modularized finite difference dynamical core (based on an Arakawa "C"-grid) [*Suarez and Takacs*, 1995] that incorporates improved tracer transport [*Hourdin and Armengaud*, 1995]. This latest version has been termed *NASA ARC Mars GCM, version 2.3* (gcm2.3). Please see *Kahre et al.* [2017] for further details on this particular release.

Results: We focus here on two multi-annual water cycle simulations: (i) one where water-ice clouds are radiatively active ("RAC" case); and, (ii) one where ice clouds are radiatively inert ("nonRAC" case). These two cases are subsets detailed in *Kahre et al.* [2017] to assess attributes of the simulated water cycle together with comparisons with recent MGS and MRO obser-
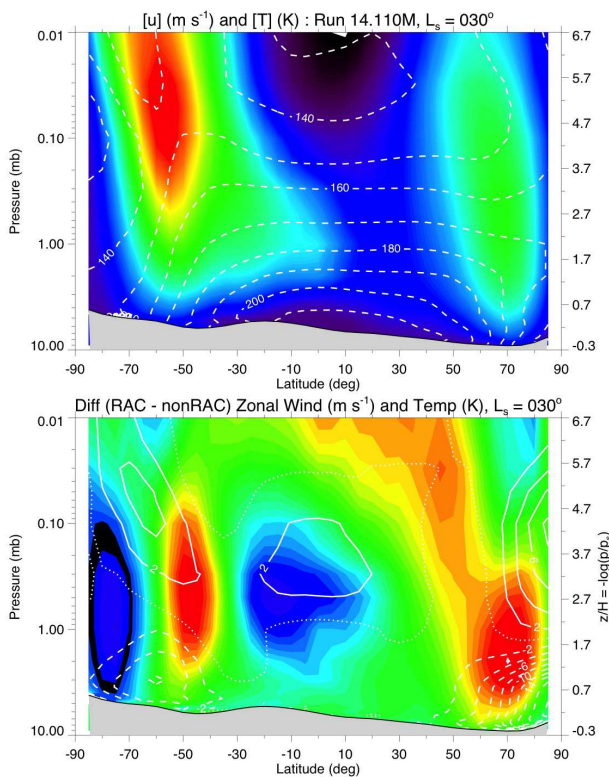
nucleation contact parameter, m).

Figure 2 shows mean zonal cross section of the zonal wind (color) and temperature (white dashed contours) during northern early spring ($L_s = 30°$) from the two simulations. In the RAC case (top panel), there is strong baroclinicity within middle and high latitudes of both northern and southern hemispheres, and strong westerly jets are indicated with maximum speeds over $110\,\mathrm{m\,s^{-1}}$. In northern midlatitudes, the mean zonal isotherms show little tilt within the first couple scale heights (i.e., they are
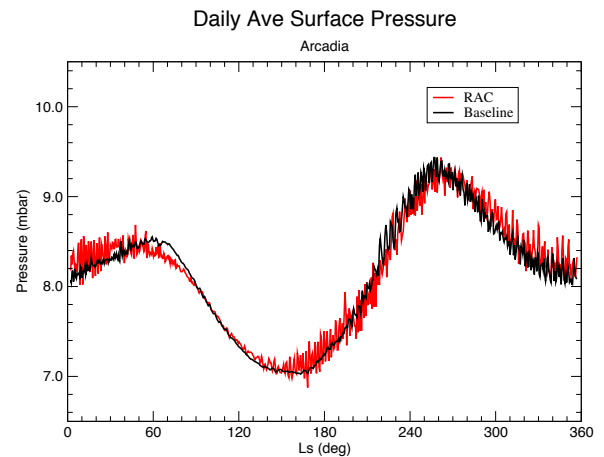

Figure 3: Daily averaged surface pressure in the Arcadia region as a function of L_s for the RAC case (red curve) and the baseline (nonRAC) case (black curve).

Figure 2: Time and zonally averaged temperature (K) and zonal wind (m s^{-1}) during early northern spring ($L_s = 30°$) for the RAC case (a) and the corresponding difference fields (i.e., RAC–nonRAC) (b) from the water cycle simulations conducted with the ARC Mars GCM. The contour interval is 10 K and 2 K in panels (a) and (b), respectively, and in (b) negative values are dashed. Color shading corresponds to zonal wind.

vations, and further, several sensitivity experiments to the assumed cloud microphysical parameters (e.g., the

more vertically oriented) than in the nonRAC case. This characteristic holds also at other seasons. Differences (i.e., RAC–nonRAC) between these two corresponding fields (bottom panel) show that radiatively-active water ice clouds profoundly affect the seasonal mean climate. There is a bulk warming of the atmosphere in the subtropics aloft, a cooling (warming) of the atmosphere in lower (upper) regions at high latitudes, and, increases in the mean pole-to-equator temperature contrasts (i.e., stronger mean "baroclinicity") resulting in augmented zonal jets. Such thermal and mean circulation changes have also been found in the studies by *Haberle et al.* [2011], *Madeleine et al.* [2014] and *Navarro et al.* [2014]. The mean overturning (i.e., "Hadley") circulation is also enhanced in the RAC case. These changes are significant in the middle and high latitudes. Comparisons with MGS/TES and MRO/MCS measurements indicate better agreement between the model's simulated climate compared to observations.

The increased baroclinicity is robust and significantly affects the intensity and seasonality of synoptic weather systems. Figure 3 shows time series of the daily-averaged surface pressure in the northern hemisphere (NH) Arcadia region, a geographic region previ-

ously found to indicate enhanced synoptic-period transient wave activity (i.e., a "storm zone") [*Hollingsworth et al.*, 1996; *Hollingsworth et al.*, 1997]. It can be seen that there is enhanced synoptic period variability (i.e., day-to-day weather) in both amplitude and intra-seasonality in the simulation with radiatively-active water ice clouds (red curve). Similar characteristics are found in the other storm zone regions of the NH. In addition, the SH extra-tropics also indicate enhanced synoptic-period variability, particularly in the western hemisphere. This result also appears to be insensitive to model (horizontal) resolution. High-resolution ($\times 2$) simulations for the RAC and baseline cases indicate very similar transient eddy amplitudes and seasonality.

As indicated in Figure 4, synoptic period variability is significantly enhanced in the RAC case. Transient-eddy poleward heat fluxes within the NH and SH extra-tropics are very much enhanced in the RAC case compared to the nonRAC case (i.e., a factor of three stronger at least). As such, the baroclinic/barotropic eastward
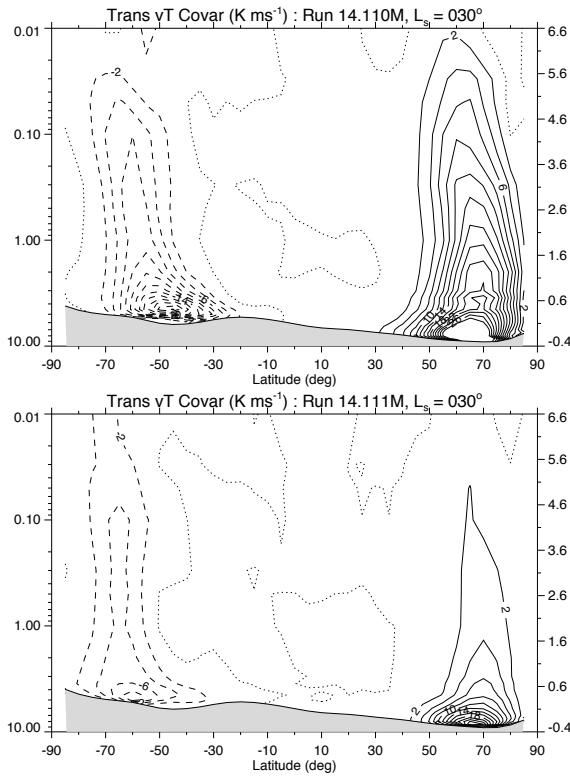

Figure 4: Transient eddy poleward heat flux (K m s^{-1}) for the RAC case (top panel) and the nonRAC case (bottom panel) during early northern spring ($L_s = 30°$). The contour interval in both panels is 2 K m s^{-1}. Positive values are solid, negative values are dashed.

traveling waves are much more efficient in transport-

ing heat, momentum and other scalar quantities (e.g., atmospheric tracers) within middle latitudes.
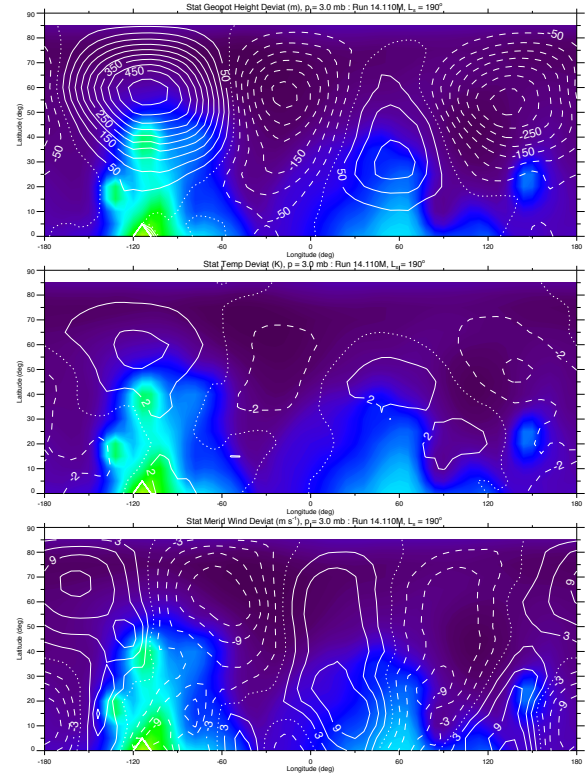

Figure 5: NH longitude-latitude cross sections during early northern autumn ($L_s = 190°$) at 3.0 mbar of stationary (a) geopotential height (m); (b) temperature (K); and, (c) meridional wind (m s^{-1}) from the Mars GCM with RAC. The above fields are shown in white contours (negative dashed) and the color shading is the smoothed topography at the resolution of the GCM.

Consideration of the stationary, forced Rossby modes within the RAC case during early NH autumn ($L_s = 190°$) in terms of a longitude-latitude section at the 3.0 mbar level are presented in Figure 5. Within the northern hemisphere, this figure presents the stationary geopotential height (top panel); temperature (middle panel); and meridional wind (bottom panel). In all three mean zonal departure fields, a clear zonal wavenumber $s = 2$ stationary pattern is evident. This is generally a robust NH pattern, and is further discussed in *Haberle et al.* [2017] for other seasons, and comparisons with MRO/MARCI UV water-ice cloud observations. What is apparent in Figure 5 is a strong correlation of the forced Rossby-wave pattern with the large-scale orography: namely, high relief collocated with high geopotential; low relief collocated with low geopotential—a classic signature of forced Rossby wave responses within a baroclinic atmo-

sphere [*Hoskins and Karoly*, 1981]. In the nonRAC case (not shown) the forced Rossby wave pattern presents a more zonal wavenumber $s = 1$ stationary pattern in middle and high latitudes, and one of much weaker amplitude in the three fields considered.

There is significant interplay between the forced Rossby stationary modes and the traveling synoptic period transient waves. In particular, the geographic "localization" of maximum band-pass transient variance is highly tied to the forced Rossby modes. Shown in Figure 6 for the RAC Mars GCM simulation during early NH autumn ($L_s = 190°$) in terms of a longitude-latitude section at the 3.0 mbar are similar fields presented in Figure 5 yet for the band-pass filtered (i.e., 2–10 day) RMS transient geopotential height (top panel); temperature (middle panel); and, meridional wind (bottom panel). The amplitude and location of the transient RMS maxima are vastly different in the RAC case versus the nonRAC case (not shown): there is localization of peak transient temperature variance just northeast of the Tharsis highlands in the RAC case whereas a more zonally uniform and weaker pattern occurs in the nonRAC case. Further, the meridional wind transient fields are much stronger in amplitude and geographically localized in the RAC case compared to the nonRAC case (not shown).

Such transient synoptic period storm zone patterns vary between the RAC and the nonRAC cases in subtle yet nontrivial ways, and the maxima and geographic localization of transient variability occur differently at the same seasons within the annual cycle.

Summary: Many upgrades to the NASA Ames Research Center (ARC) Mars global climate model (GCM) have occurred recently and include a modern radiative transfer package and cloud microphysics package that permit radiative effects and interactions of suspended atmospheric aerosols (e.g., water ice clouds, water vapor, dust, and their mutual interactions) to influence the net diabatic heating within the atmosphere. Atmospheric aerosols are critically important in determining the nature of the mean thermal structure and circulation, and hence the overall climate of the planet [*Hobbs*, 1993].

Our Mars GCM simulations indicate that radiatively active ice clouds profoundly affect the seasonal and annual mean climate in a variety of ways. Such results suggest that the bulk thermal structure and resultant circulation patterns are strongly modified near the surface and aloft. Generally speaking, it is found there is warming of the atmosphere in subtropical and high-latitude upper layers, cooling of the atmosphere in the lower high-latitude regions, and, increases in the mean pole-to-equator temperature contrasts (i.e., stronger mean "baroclinicity") and augmented zonal jets. Comparisons with MGS/TES and MRO/MCS measurements show better agreement between the model's simulated climate compared to that observed. An increased baroclinicity significantly affects the intensity and seasonality of synoptic weather systems.
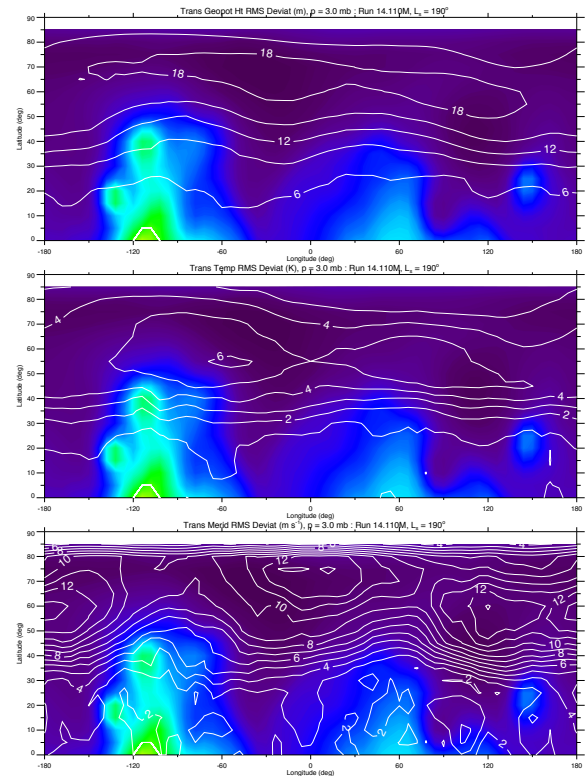

Figure 6: NH longitude-latitude cross sections during early northern autumn ($L_s = 190°$) at 3.0 mbar of transient band-pass filtered RMS (a) geopotential height (m); (b) temperature (K); and, (c) meridional wind (m s^{-1}) from the Mars GCM with RAC. The above fields are shown in white contours and the color shading is the smoothed topography at the resolution of the GCM.

References:

Banfield et al., 2004: *Icarus*, **170,** 365; Barnes et al., 1993: *J. Geophys. Res.*, **98,** 3125; Haberle et al., 2011: *MAMO4*, Paris, France; Haberle et al., 2017: In prep; Hobbs, 1993: *Aerosol-Cloud-Climate Interactions*, Academic Press; Hollingsworth et al., 1996: *Nature*, **380,** 413; Hollingsworth et al., 1997: *Adv. Space Res.*, **19,** 1237; Hoskins and Karoly, 1981: *J. Atmos. Sci.*, **38,** 1179; Hourdin and Armengaud, 1995: *Mon. Wea. Rev.*, **127,** 822; Kahre et al., 2017: *MAMO6*, Granda, Spain; Lacis and Oinas, 1991: *J. Geophys. Res.*, **96,** 9027; Madeleine et al., 2014: *Geophys. Res. Lett.*, **41,** 4873; Mellor and Yamada, 1982: *Rev. Geophys. Space Phys.*, **20,** 851; Montmessin et al., 2002: *J. Geophys. Res.*, **106,** E65037; Montmessin et al., 2004: *J. Geophys. Res.*, **109,** E10004; Navarro et al., 2014: *J. Geophys. Res.*, **119,** 1479; Suarez and Takacs, 1995: NASA Tech. Memo. 104606; Toon et al., 1989: *J. Geophys. Res.*, **94,** 16287; Wang et al., 2005: *J. Geophys. Res.*, **110,** E07005.